Schizophrenia Bulletin vol. 46 no. 6 pp. 1426–1438, 2020
doi:10.1093/schbul/sbaa097
Advance Access publication 3 August 2020

Latent Clinical-Anatomical Dimensions of Schizophrenia

Matthias Kirschner[†,1,2], Golia Shafiei[†,2], Ross D. Markello[2], Carolina Makowski[2], Alexandra Talpalaru[3,4], Benazir Hodzic-Santor[2], Gabriel A. Devenyi[3,5], Casey Paquola[2], Boris C. Bernhardt[2], Martin Lepage[3,5], M. Mallar Chakravarty[3–5], and Alain Dagher[†,2], Bratislav Mišić[*,†,2]

[1]Department of Psychiatry, Psychotherapy and Psychosomatics, Psychiatric Hospital, University of Zurich, Zurich, Switzerland; [2]McConnell Brain Imaging Centre, Montréal Neurological Institute, McGill University, 3801 Rue University, Montreal H3A 2B4, Canada; [3]Cerebral Imaging Center, Douglas Mental Health University Institute, McGill University, Montréal, Canada; [4]Department of Biological and Biomedical Engineering, McGill University, Montréal, Canada; [5]Department of Psychiatry, McGill University, Montréal, Canada

*To whom correspondence should be addressed; tel: 514-398-1857, fax: 514-398-1857, e-mail: bratislav.misic@mcgill.ca
[†]These authors contributed equally to this work.

Widespread structural brain abnormalities have been consistently reported in schizophrenia, but their relation to the heterogeneous clinical manifestations remains unknown. In particular, it is unclear whether anatomical abnormalities in discrete regions give rise to discrete symptoms or whether distributed abnormalities give rise to the broad clinical profile associated with schizophrenia. Here, we apply a multivariate data-driven approach to investigate covariance patterns between multiple-symptom domains and distributed brain abnormalities in schizophrenia. Structural magnetic resonance imaging and clinical data were derived from one discovery sample (133 patients and 113 controls) and one independent validation sample (108 patients and 69 controls). Disease-related voxel-wise brain abnormalities were estimated using deformation-based morphometry. Partial least-squares analysis was used to comprehensively map clinical, neuropsychological, and demographic data onto distributed deformation in a single multivariate model. The analysis identified 3 latent clinical-anatomical dimensions that collectively accounted for 55% of the covariance between clinical data and brain deformation. The first latent clinical-anatomical dimension was replicated in an independent sample, encompassing cognitive impairments, negative symptom severity, and brain abnormalities within the default mode and visual networks. This cognitive-negative dimension was associated with low socioeconomic status and was represented across multiple races. Altogether, we identified a continuous cognitive-negative dimension of schizophrenia, centered on 2 intrinsic networks. By simultaneously taking into account both clinical manifestations and neuroanatomical abnormalities, the present results open new avenues for multi-omic stratification and biotyping of individuals with schizophrenia.

Key words: schizophrenia/negative symptoms/functional MRI/structural MRI/transdiagnostic models/addiction

Introduction

Schizophrenia is characterized by heterogeneous clinical manifestations, including positive symptoms, negative symptoms, and generalized cognitive impairments. This complex clinical pattern is already prevalent prior to and during first-episode psychosis.[1] While positive symptoms tend to reduce over time, negative and cognitive symptoms are more likely to persist over time, severely affecting long-term social functioning and quality of life.[2–9]

Convergent findings from neuroimaging link clinical manifestations of schizophrenia with widespread disruption of structural and functional brain networks.[10–13] Several large-scale studies and meta-analyses provide evidence for widespread anatomical alterations, including reduced cortical thickness, subcortical volume, and white matter integrity.[14–16] These localized brain abnormalities have individually been linked to clinical manifestations of positive, negative, and cognitive symptoms.[17–20]

But how do complex clinical phenotypes map onto distributed brain networks? The organization of brain connectivity increases the likelihood that local pathological perturbations affect synaptically connected neuronal populations.[21] Thus, structural abnormalities with a distributed topography may reflect the underlying network architecture and manifest as a diverse set of cognitive and affective symptoms.[22–25] Recent studies have demonstrated such links between brain structure and function both in healthy controls[26,27] and across a number of neurological and psychiatric diseases.[28–32]

Several methodological limitations might have hampered the progress to identify comprehensive clinical-anatomical signatures of schizophrenia. First, the heterogeneity of clinical manifestation cannot be captured by case-control designs or studies focusing on a single-symptom domain (eg, only positive or only negative symptoms). Second, many previous studies were designed to capture associations between symptom dimensions and global brain measures or localized brain changes with a priori defined regions of interest. Altogether, previous work eschews the possibility of a pleiotropic-like mapping between anatomy and function, whereby distributed structural alterations may simultaneously lead to multiple positive and negative symptoms.[17–20,33]

The relationship between anatomical abnormalities and clinical manifestation is particularly important for understanding heterogeneity in the patient population. Recent efforts have been directed toward stratifying individuals into nonoverlapping clusters or biotypes based either on clinical-behavioral features[34] or neuroimaging features.[35] Although promising, such "hard partitioning" methods are designed for precise categorical stratification based either on clinical/behavioral or neuroimaging measures but do not consider the possibility of continuous phenotypic dimensions that span multiple clinical domains, nor do they explicitly integrate clinical and neuroanatomical features. By focusing on single "modalities" (clinical only or imaging only), unsupervised learning methods miss out on the critical link between brain and behavior and may yield solutions that are difficult to interpret or reconcile with clinical experience.[30] Thus, identifying continuous clinical-anatomical dimensions would complement categorical biotyping efforts, helping to situate individuals and biotypes in a wider multivariate space defined by both clinical presentation and anatomical abnormalities.[36,37]

Here we apply a data-driven method to identify multimodal phenotypic axes of schizophrenia. Specifically, we use a multivariate mapping between whole-brain anatomical alterations and clinical domains in schizophrenia to reveal latent clinical-anatomical dimensions. In the present work, clinical dimensions comprise positive and negative symptoms (based on clinical ratings) and cognitive impairments (based on neurocognitive testing) following the dimensional framework from van Os and Kapur[38,39] and current conceptualizations of the Diagnostic and Statistical Manual of Mental Disorders (DSM)-5 and the International Classification of Diseases (ICD)-11[40,41]. We first estimate gray matter abnormalities in a sample of $n = 133$ individuals with chronic schizophrenia and $n = 113$ healthy controls from the Northwestern University Schizophrenia Data and Software Tool (NUSDAST; http://schizconnect.org).[42] Deformation-based morphometry (DBM) was applied to T1-weighted MR images to estimate cortical and subcortical gray matter tissue volume loss in patients with schizophrenia relative to healthy controls (hereafter referred to as "deformation").[43–48] We then

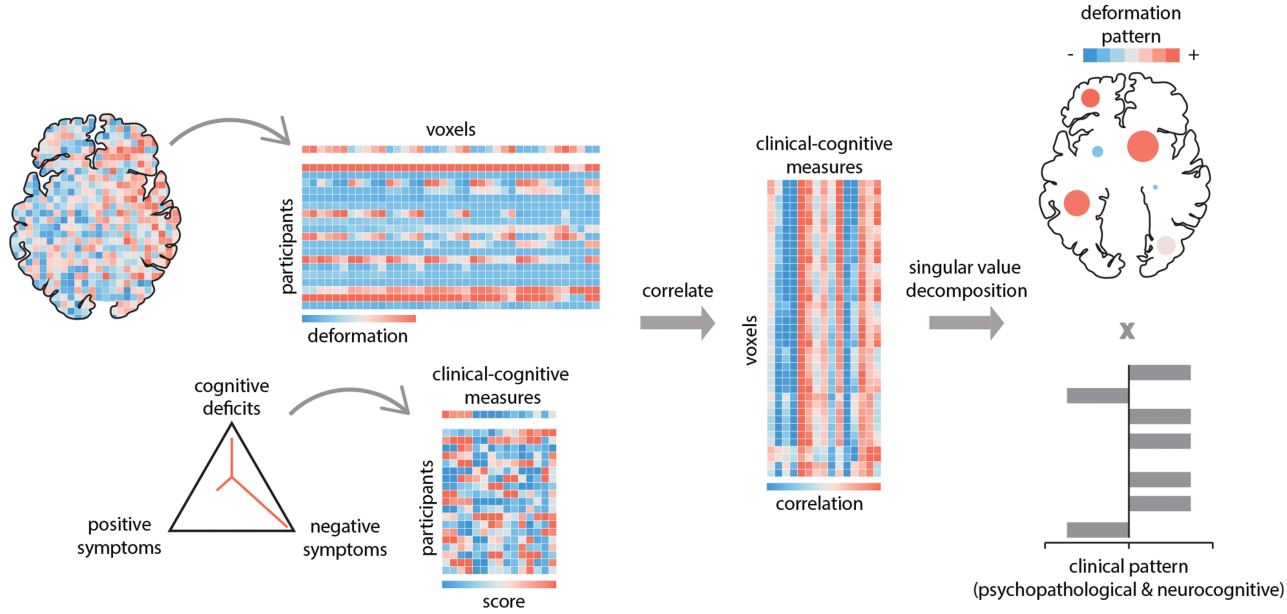

Fig. 1. Partial least-squares (PLS) analysis is a form of reduced-rank regression used to relate two sets of variables to each other. The original variables are correlated across participants and subjected to singular value decomposition. The decomposition yields multiple latent variables: linear combinations of the original variables, with the weights chosen to maximize the covariance between them. The contribution of individual variables to the latent variable is assessed by bootstrap resampling. The pairing of the deformation and clinical-cognitive pattern is assessed by permutation tests and cross-validation. Clinical dimensions adapted from van Os and Kapur[38] and follow current conceptualizations of the DSM-5 and ICD-11[40,41]. In the present study, data for the following clinical dimensions were available: positive symptoms, negative symptoms, and cognitive impairments.

identify disease-related deformation patterns using partial least-squares (PLS) analysis (figure 1).[49–51] The technique isolates patterns of deformation directly related to multiple-symptom dimensions (including positive, negative, and cognitive symptoms) and demographic data (table 1). We first validate the results in an independently collected data set. We then investigate whether the spatial patterning of deformation is related

Table 1. Sample characteristics. Clinical, behavioral and demographic characteristics. (A) Discovery sample (Northwestern University Schizophrenia Data and Software Tool [NUSDAST]). (B) Validation sample (Douglas Institute)

(A) Discovery data (NUSDAST)	SCZ (n = 133)	HC (n = 113)	Statistic
Age, mean (SD)	34.8 (13.2)	23.5 (8.4)	t = 7.85**
Female sex, no. (%)	48 (36.1)	64 (56.6)	x^2 = 10.48*
Years in school, mean (SD)	12.2 (2.3)		
Age of onset, mean (SD)[a]	21.6 (8.0)		
Years illness duration, mean (SD)[a]	12.9 (12.5)		
SES score, mean (SD)	45 (15.5)		
WMS cognitive, mean (SD)	−0.00005 (4.9)		
WAIS score, mean (SD)			
Matrix	8.9 (3.3)		
Vocabulary	7.9 (3.6)		
ESRS score, mean (SD)			
Global	1.2 (1.9)		
Total	5.5 (6.6)		
SANS score, mean (SD)			
Avolition/apathy	10.7 (6.9)		
Avolition/apathy—global	4.3 (2.4)		
Diminished expression	10.3 (9.5)		
Diminished expression—global	3.0 (2.2)		
SAPS score, mean (SD)			
Disorganization	5.1 (5.8)		
Disorganization—global	1.8 (1.7)		
Reality distortion	13.5 (12.7)		
Reality distortion—global	3.2 (2.5)		
Chlorpromazine equivalent dosage, mean (SD)[b]	391.3 (379.8)		
Information on medication status obtained, no. (%)[c]	93.2		
Type of medication, %[c]			
Typical	12.9		
Atypical	70.2		
Both	12.2		
Unmedicated	4.8		
(B) Validation data (Douglas Institute)	**SCZ (n = 108)**	**HC (n = 69)**	**Statistic**
Age, mean (SD)	35.2 (8.2)	34.1 (9.0)	t = 0.84
Female sex, no. (%)	26 (24.0)	21 (30.4)	x^2 = 0.87
WASI full-scale IQ, mean (SD)	95.23 (14.58)		
Cognitive composite score, mean (SD)[d]	−5.5 (5.6)		
SANS score, mean (SD)			
Avolition/apathy	12.3 (7)		
Avolition/apathy—global	5.8 (2.1)		
Diminished expression	10.3 (7.1)		
Diminished expression—global	3.7 (2.0)		
SAPS score, mean (SD)			
Disorganization	5.6 (6.5)		
Disorganization—global	2.4 (2.1)		
Reality distortion	12.8 (13.7)		
Reality distortion—global	4.2 (3.1)		
Chlorpromazine equivalent dosage, mean (SD)	798.3 (825.3)		

Note: SCZ, schizophrenia; HC, healthy control; SES, socioeconomic status; WMS, Wechsler Memory Scale; ESRS, Extrapyramidal Symptom Rating Scale; SANS, Scale for the Assessment of Negative Symptoms; SAPS, Scale for the Assessment of Positive Symptoms.
[a]Based on 131 patients.
[b]Based on 86 patients.
[c]Based on 124 patients.
[d]Normalized composite cognitive score estimated from the CogState Research Battery protocol that includes cognitive domains of verbal memory, visual memory, working memory, processing speed, executive function, visual attention, and social cognition.
*< .01, **< .001

to the intrinsic functional architecture of the brain. Finally, we link the most reliable clinical-anatomical dimensions to broader societal variables of interest, including socioeconomic status (SES) and race.

Methods

Discovery Data set: NUSDAST

The discovery data set was derived from the NUSDAST,[42] downloaded from XNAT Central (http://central.xnat.org/) and the SchizConnect data-sharing portal (http://schizconnect.org/). Briefly, the NUSDAST data set is a cohort of individuals with schizophrenia, their nonpsychotic siblings, healthy controls, and their siblings. Detailed information is available at [42]. The final data set used in this study comprised 133 individuals with schizophrenia and 113 healthy controls. Detailed inclusion criteria are included in the supplementary methods, while the selection flowchart is shown in supplementary figure S1.

NUSDAST Clinical and Neurocognitive Data

Clinical and demographic data were derived from the baseline visit provided by the NUSDAST database (table 1). Among the demographic measures, we used age, sex/gender, years of schooling, and SES. The clinical assessment included the Scale for the Assessment of Positive Symptoms (SAPS[52]) and the Scale for the Assessment of Negative Symptoms (SANS[53]). Following the 4 symptom dimensions approach from Kotov et al,[54] as well as Strauss et al (for 2 negative symptom factors, respectively),[55] we calculated 2 negative symptom factors and 2 positive symptom factors. The 2 negative symptom dimensions comprised the SANS diminished expression factor (including affective flattening, alogia) and the SANS avolition–apathy factor (including avolition and anhedonia). The 2 positive symptom dimensions comprised the SAPS reality distortion factor (including hallucinations and delusions) and the SAPS disorganization factor (including bizarre behavior and thought disorder). These 4 factors were calculated for individual items (sum scores) and global ratings separately, resulting in a total of 8 factors. Furthermore, total and global scores of the Extrapyramidal Symptom Rating Scale were included to assess 4 types of drug-induced movement disorders (DIMD) caused by antipsychotic treatment: parkinsonism, akathisia, dystonia, and tardive dyskinesia.[56,57]

Overall cognitive functioning was assessed with a composite score following the method suggested by Czepielewski et al.[18] The composite score (WMS Cog) included the sum of the *z*-transformed scores on Logical Memory, Family Pictures, Letter-Number Sequencing, Spatial Span, and Digit Span from the Wechsler Memory Scale (WMS-III[58]). Finally, individual scaled scores from the WAIS-III Matrix Reasoning and Vocabulary subsets were included as measures of executive function[42] and crystallized knowledge (ie, premorbid crystallized intellectual functioning[18]), respectively. Altogether, 15 demographic, clinical, and neurocognitive measures were entered in the PLS analysis to identify latent clinical-anatomical dimensions related to multiple-symptom dimensions. Please note that, in the present work, cognitive deficits are defined as a clinical dimension following the current conceptualizations of the DSM-5 and ICD-11[40,41]. This approach should be distinguished from research investigating cognition in a biomarker framework of schizophrenia.[34,59,60] SES, age of onset, duration of illness, and antipsychotic medication (chlorpromazine equivalents) were left out from the PLS analysis and their relation with the final statistical model (clinical-anatomical dimensions) was tested post hoc (for details see supplementary methods).

NUSDAST Neuroimaging Data

All magnetic resonance imaging (MRI) scans were acquired on the same 1.5 T Vision scanner platform (Siemens Medical Systems) at the Mallinckrodt Institute of Radiology at Washington University School of Medicine.[42] Automated preprocessing was performed using the minc-bpipe-library pipeline (https://github.com/CobraLab/minc-bpipe-library) following manual quality control to remove scans with insufficient quality; see supplementary methods. Local change in the brain tissue's volume density was calculated using DBM[61]. We interpret regional DBM values as measures of tissue loss or tissue expansion.[43–47] Note, however, that morphometric techniques do not directly measure the underlying cellular morphology and constitute a statistical model of physiological changes. DBM is estimated based on the deformation applied at each voxel to nonlinearly register each brain to a given template. For details of the DBM pipeline, please see supplementary methods. Chronological age was regressed from DBM values prior to PLS analysis in both the NUSDAST and Douglas data sets.

Validation Data Set: Douglas Institute

T1-weighted MRI scans of 108 individuals with schizophrenia and 69 healthy controls were obtained from an independently collected data set to validate the original findings (table 1). Details about the participant inclusion criteria, MRI acquisition, and data preprocessing are available elsewhere[62] and also described in the supplementary information. Regional DBM values and clinical-cognitive measures overlapping with the discovery set were used for further analysis.

Partial Least Squares

We used PLS analysis to investigate the relationship between local changes in deformation (DBM values) and

clinical-cognitive measures (figure 1). PLS analysis is a multivariate statistical technique that identifies weighted patterns of variables in 2 given sets or data blocks that maximally covary with each other.[49–51] In the present analysis, 1 variable set corresponded to deformation and the other to clinical-cognitive measures. The 2 variable sets were correlated with each other across patients, and the resulting correlation matrix was subjected to singular value decomposition to identify latent clinical-anatomical dimensions.

Inference and validation of the statistical model were performed using nonparametric methods: (1) statistical significance of overall patterns was assessed by permutation tests[63]; (2) feature (voxel, clinical-cognitive measure) importance was assessed by bootstrap resampling[64]; (3) out-of-sample correlations between projected scores were assessed by cross-validation[65]; (4) stability of deformation and clinical-cognitive patterns was assessed by split-half resampling.[66] Mathematical details of the analysis and inferential methods are described in supplementary methods and results.

Results

Clinical-Anatomical Dimensions of Schizophrenia

Multivariate PLS analysis identified 3 statistically significant latent variables (LVs) that represent pairings between distributed deformation patterns (estimated by age-corrected DBM) and clinical-cognitive measures (figure 2a; LV-1: permuted $P = 7.3 \times 10^{-3}$; LV-2: permuted $P = 5 \times 10^{-4}$; LV-3: $P = 7 \times 10^{-4}$). These patterns respectively account for 27.5%, 15%, and 13% (total of 55.5%) of the covariance between clinical-cognitive data and brain deformation. Based on effect size and reliability (see below), we focus on LV-1 in the main text.

Figure 2b shows the loadings (ie, correlations) of individual clinical and cognitive scales with the first latent variable (LV-1). The strongest contributors to LV-1 were cognitive deficits (all $r < -.45$), severity of negative symptoms (all $r > .38$), and educational attainment ($r = -.45$). Positive symptoms and DIMD also contributed to LV-1 but to a lesser extent (all $r > .15$ but $< .2$). In other words, LV-1 captures predominantly clinical features of the cognitive and negative symptom domains (cognitive-negative dimension).

Figure 2c shows the corresponding deformation pattern associated with LV-1, indexed by bootstrap ratios. Briefly, bootstrap ratios measure the reliability of each weight across participants and can be interpreted as a z-score (see supplementary methods for more detail). This brain deformation pattern is comprised of occipital (visual), medial parietal, lateral temporal, prefrontal (medial prefrontal cortex and superior frontal gyrus), limbic, and paralimbic regions, including the cingulate (anterior and posterior) and hippocampus. In addition, the deformation pattern involves subcortical regions, including the caudate and cerebellar structures. Altogether, the first latent clinical-anatomical dimension indicates that distributed deformation in this distributed network of regions is associated with negative symptom severity and lower cognitive performance. Finally, clinical and deformation scores were then correlated (figure 2d); the mean out-of-sample correlations were $r = .27$ (figure 2e). Further details on cross-validation in supplementary results.

LV-2 and LV-3 are shown and described in detail in the supplementary results (supplementary figures S2b and S2c). Associations between patient-specific scores of all 3 latent variables and age of onset, duration of illness, and medication dosage are reported in supplementary results.

External Replication

To further assess the reliability of the results, we validated the PLS-derived patterns in an independently acquired replication data set (Douglas data set; $n = 108$ individuals with schizophrenia; see Methods). Regional DBM values from the validation set (Douglas) were projected onto the PLS model derived from the discovery set (NUSDAST) to estimate the predicted brain deformation scores for the validation set. The predicted brain deformation scores were then correlated with the 12 clinical, cognitive, and demographic measures that were common to 2 data sets, yielding a predicted clinical profile for the validation set (supplementary figure S3, left column). The discovery and validation clinical profiles were then correlated, and the significance of correlations was tested against a permuted null model (1000 repetitions; supplementary figure S3, middle column). Finally, bootstrap resampling was used to generate a distribution of correlations between the discovery and validation profiles (1000 repetitions; supplementary figure S3, right column).

For LV-1 (cognitive-negative dimension), we find a significant association between the clinical profiles of the discovery and validation data sets ($r = .6$, $P = 2.0 \times 10^{-2}$; 95% CI: [0.09 0.90]; supplementary figure S3). In other words, projecting the brain deformation data from the validation set on LV-1 of the discovery revealed a similar cognitive-negative clinical profile with 36% of variance explained. Thus, we were able to partly replicate the clinical-anatomical dimension of LV-1 in an independent validation data set. Repeating the same analysis for LV-3 revealed a positive but nonsignificant association between the clinical profiles of the discovery and validation data sets ($r = .42$, $P = 1.09 \times 10^{-1}$; 95% CI: [−0.60 0.92]) and no significant association between the clinical profiles of LV-2 ($r = -.50$, $P = 5.8 \times 10^{-2}$; 95% CI: [−0.87 0.26]). Please note that the discovery (NUSDAST) and replication data set (Douglas) differed significantly in several aspects, including ethnicity (NUSDAST: mixed Caucasian and African-American, Douglas: Caucasian), fewer female participants ($\chi^2 = 4.04$, $P = 4.4 \times 10^{-2}$), higher antipsychotic medication ($t = 4.49$, $P < 1.0 \times 10^{-4}$) and higher global positive and negative symptoms in the discovery sample (SAPS Disorganization Global, $t = 2.38$, $P = 1.8 \times 10^{-2}$; SAPS RealityDistortion Global,

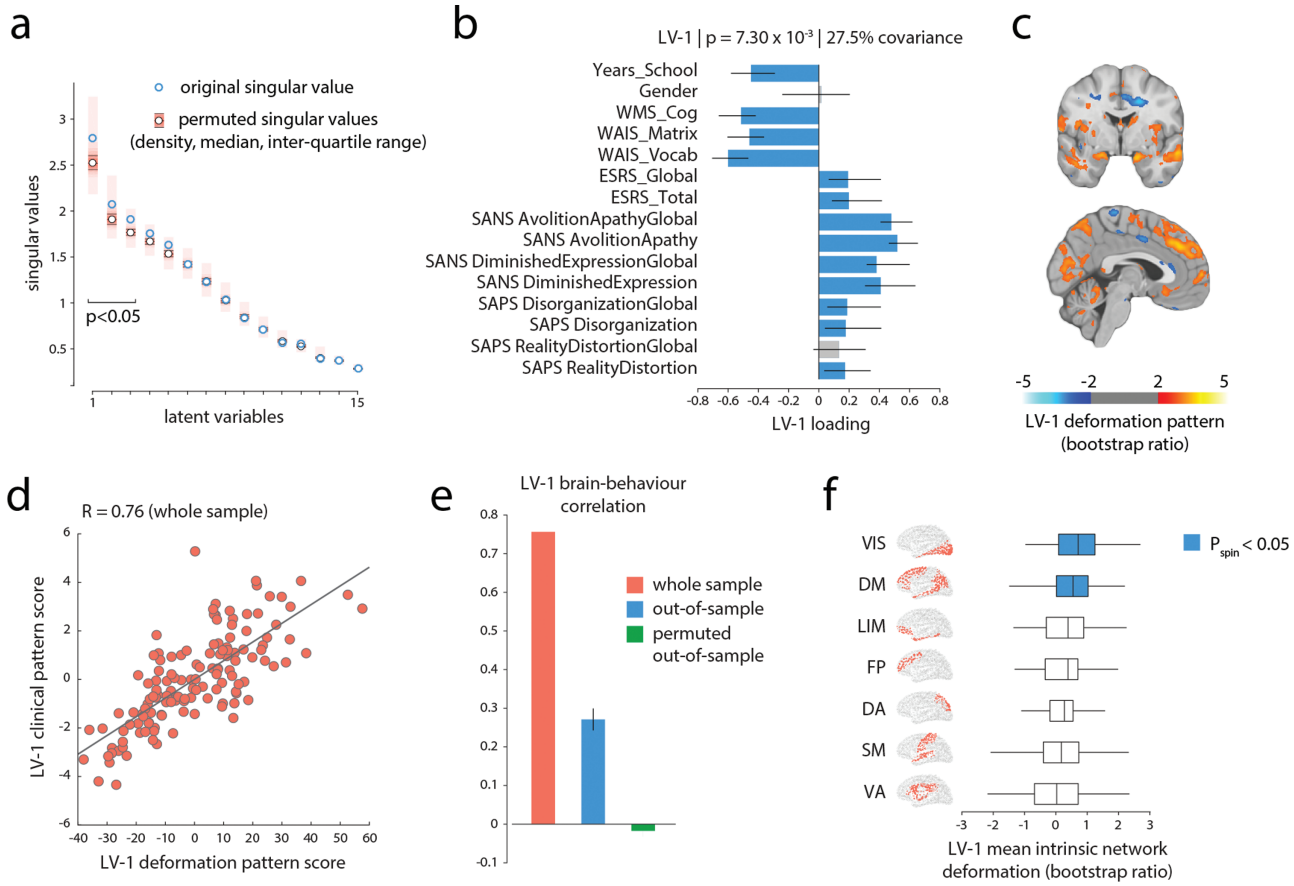

Fig. 2. A clinical-anatomical signature of schizophrenia. (a) Partial least-squares (PLS) analysis detected 3 statistically significant latent variables, mapping distributed patterns of deformation to clinical-cognitive characteristics. The first latent variable (LV-1) accounted for 27.5% of the covariance between the MRI and clinical-cognitive data. (b) Clinical features of LV-1. The contribution of individual clinical cognitive measures is shown using correlations between patient-specific clinical scores and scores on the multivariate pattern (loadings). Error bars indicate bootstrap-estimated SEs. (c) LV-1 deformation pattern. The contribution of individual voxels is shown using bootstrap ratios (ratios between voxel weights and bootstrap-estimated SEs, interpretable as *z*-scores; see supplementary methods for more detail). The deformation pattern is displayed on an MNI template (MNI152_symm_2009a; $x = -3$, $y = -2$). Patients who display this deformation pattern tend to score higher on measures of clinical severity of negative symptoms (eg, SANS Avolition–Apathy) and tend to score lower on cognitive measures (eg, WAIS). (d) Individual patient data is projected onto the weighted patterns shown in (b) and (c) to estimate scalar patient scores that quantify the extent to which individual patients express each pattern in LV-1. The 2 scores are correlated, suggesting that patients who display the deformation pattern in (c) tend to express the clinical phenotype in (b). (e) Correlations between deformation and clinical scores in the original sample (left; same as panel d), in held-out data (middle), and in a permuted null (right). (f) Specific intrinsic-network deformation. The PLS-derived deformation pattern is stratified into resting-state networks (RSNs) defined by Yeo et al[68]. The bars indicate mean deformations for each network. *P*-values are estimated with respect to the spin test null developed by Alexander-Bloch et al[67]. Yeo networks: DM = default mode, DA = dorsal attention, VIS = visual, SM = somatomotor, LIM = limbic, VA = ventral attention, FP = fronto-parietal.

$t = 2.55$, $P = 1.1 \times 10^{-2}$; SANS Avolition–Apathy Global, $t = 2.75$, $P = 6.0 \times 10^{-3}$; SANS Diminished Expression Global, $t = 2.55$, $P = 1.1 \times 10^{-2}$). Although these marked differences might have hampered the replication of all 3 clinical-anatomical dimensions, the most prominent clinical profile of the LV-1 is still represented in the independent replication data set.

Clinical-Anatomical Dimensions Map on Intrinsic Networks

We next asked how clinically defined deformation patterns are topographically distributed in the brain and whether their organization reflects the underlying functional architecture. The deformation pattern corresponding to the clinical features of LV-1 (cognitive-negative dimension) appears to mainly target brain regions associated with the default mode network and visual network (figure 2c). To statistically assess if this is the case, we used a recently developed spatial permutation procedure.[67] We stratified voxels according to their membership in 7 intrinsic networks and calculated the mean bootstrap ratio value within each network.[68] To construct a null distribution for network means, we projected the data on a sphere and randomly rotated the sphere, permuting the intrinsic-network labels of brain regions but preserving the spatial autocorrelation of the map.[67,69] The mean bootstrap ratio was then recalculated for each network for the permuted

sample. The procedure was repeated 10 000 times to construct a distribution of network means under the null hypothesis that regional volume loss patterns are independent of affiliation with specific intrinsic networks.

Figure 2e shows the mean bootstrap ratios for each network. Consistent with the voxel-wise anatomical pattern in figure 2c, deformation of the cognitive-negative dimension (LV-1) was significantly greater in the default mode and visual networks than expected by chance ($P = 1.2 \times 10^{-2}$ and $P = 3.5 \times 10^{-2}$, respectively), demonstrating a specific spatial mapping within these 2 intrinsic networks. Complete results for network specificity of deformation patterns of LV-2 and LV-3 are presented in the supplementary results and supplementary figure S2 (right column).

Clinical-Anatomical Dimensions Are Associated With Lower SES

In schizophrenia, SES is a predictor for increased risk of hospitalization,[70,71] symptom severity,[72,73] and poor outcome[74,75] and has been shown to be associated with brain function and structure.[76,77] Using simple correlations, we investigated the relation between the clinical features and corresponding deformation patterns of the first clinical-anatomical dimension with SES. We observed that both brain deformation and clinical features of LV-1 were associated with SES (anatomical: $r = .36, P = 1.8 \times 10^{-05}$, 95% CI [0.20, 0.50], clinical-cognitive: $r = .28, P = 1.0 \times 10^{-03}$, 95% CI [0.11, 0.43]). To illustrate this association, we colored the individual points, corresponding to patients, according to their SES (figure 3a). Taken together, the clinical-anatomical signature of the cognitive-negative dimension is associated with lower SES.

We next used mediation analysis (details in supplementary results) to ask whether the brain deformation pattern of LV-1 mediates the effect of SES on the corresponding clinical outcome (symptom severity; figure 3b). Unstandardized parameter estimates and SE for the model are shown in figure 3b. Regressing the PLS-derived brain deformation pattern on SES showed that lower SES is significantly associated with decreased brain volume (*a*; figure 3b). Regressing clinical expression (LV-1) on the brain deformation pattern (LV-1) showed a significant effect of brain deformation on clinical expression (*b*). However, the direct effect of SES on clinical expression (*c*) did not remain significant after the deformation pattern was modeled as a mediator (*c*′; figure 3b). In contrast, the LV-1 brain deformation pattern significantly mediates the effect of SES on clinical expression ($a \times b$; figure 3b). Taken together, the mediation analysis reveals an indirect-only mediation (mediated effect $a \times b$) with brain deformation as mediator. In other words, the severity of brain abnormalities mediates the effect of lower SES on clinical expression of the cognitive-negative dimension.

As SES is often confounded with race, we stratified patients into Caucasian and African-American and directly compared their clinical and deformation scores. Supplementary figure S4a suggests that African-American patients tend to have greater LV-1

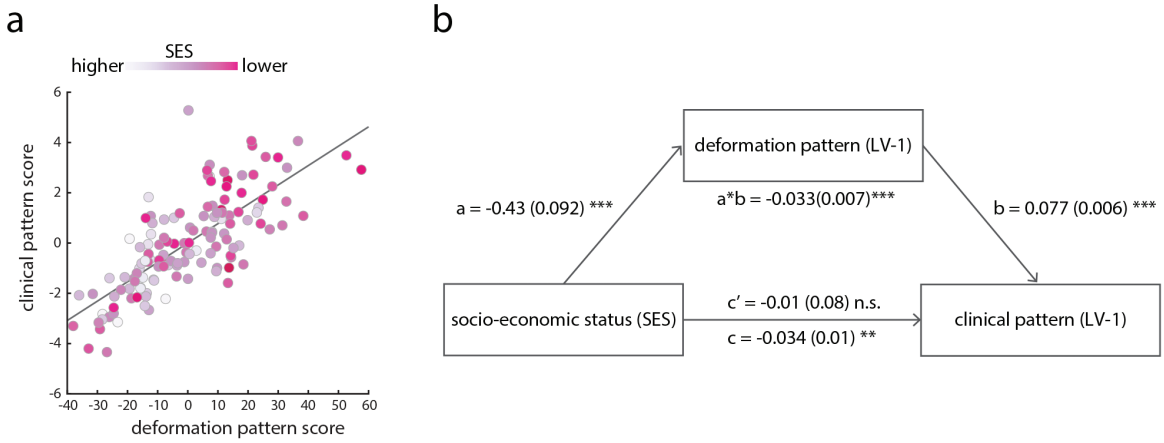

Fig. 3. Mediation analysis. (a) Correlations between patient-specific scores on the deformation and clinical-cognitive patterns in LV-1 (shown previously in figure 2d). Individual points (representing individual patients) are colored (grayscale) by their socioeconomic status (SES); individuals with lower SES tend to score more highly on both patterns. (b) Mediation analysis testing the hypothesis that the effect of SES on clinical-cognitive outcome is mediated by neuroanatomical changes. Regressing the PLS-derived brain deformation pattern on SES showed that lower SES is significantly associated with decreased brain volume ($a = -0.43$ (0.092); $P < 1.0 \times 10^{-4}$; 95% CI [−0.62, −0.24]). Regressing clinical expression (LV-1) on the brain deformation pattern (LV-1) and SES showed a significant effect of brain deformation on clinical expression ($b = 0.077$ (0.06); $P < 1.0 \times 10^{-1}$; 95% CI [0.065, 0.089]). However, the direct effect of SES on clinical expression ($c = -0.034$ (0.01); $P < 1.0 \times 10^{-2}$; 95% CI [−0.05, −0.01]) did not remain significant after the deformation pattern was modeled as a mediator ($c' = -0.001$ (0.008); $P = 0.9$; 95% CI [−0.016, 0.014]). In contrast, the LV-1 brain deformation pattern significantly mediates the effect of SES on clinical expression ($a \times b = -0.033$ (0.007); $P < 1.0 \times 10^{-1}$; 95% CI [−0.049, −0.018]).

clinical and deformation scores, but that this is mainly explained by differences in SES (2-sample t-test: $t(131) = 3.70$, $P = 3.15 \times 10^{-4}$; significantly lower SES for African-American patients). Critically, the relationship between brain deformation and clinical scores can be observed in each group separately (supplementary figure S4a; $r = 0.76, P = 5.03 \times 10^{-13}$ and $r = 0.69, P = 4.00 \times 10^{-11}$ for Caucasian and African-American patients, respectively). Moreover, the 2 correlation coefficients were not significantly different (Fisher's test, $Z = 0.83$, $P = .41$), suggesting that the first clinical-anatomical dimension remains a viable measure across different races.

Discussion

In the present report, we used multivariate mapping of comprehensive clinical-cognitive features and voxel-wise brain deformation to isolate latent clinical-anatomical dimensions of schizophrenia. Three latent clinical-anatomical dimensions were identified, collectively accounting for 55% of brain-behavior covariance, but only the first (27%) was replicated in an independent data set. This clinical-anatomical dimension encompassed cognitive deficits and negative symptoms and mapped onto a distributed brain deformation pattern centered on the default mode and visual networks. Brain deformation of this cognitive-negative dimension was represented across different races but was more pronounced in patients with lower SES. These findings suggest that a considerable population variance in schizophrenia can be described by a compact set of continuous multimodal phenotypic axes, mainly shaped by cognitive-negative symptoms and network-specific anatomical abnormalities.

Multimodal Heterogeneity of Schizophrenia

Understanding the heterogeneity of clinical and anatomical manifestations of schizophrenia remains a major challenge in schizophrenia research.[31] Numerous studies have investigated single-symptom domains in relation to either global measures (eg, total brain volume and global cortical thickness)[15,18,19] or localized brain abnormalities in predefined regions of interest.[17,20] And yet, symptom domains in schizophrenia often occur simultaneously (eg, secondary negative symptoms due to positive symptoms and/or depression,[78,79]) and are highly correlated (eg, cognitive deficits and negative symptoms,[80–82]). Likewise, brain abnormalities covary across structurally and functionally connected regions.[22,23] In the present report, we take a step toward a more comprehensive and multimodal understanding of the disease. Using a single integrative analysis, we find that the complex constellation of clinical-cognitive and anatomical features can be parsimoniously summarized by a smaller set of latent clinical-anatomical dimensions. In doing so, we derive continuous, multimodal markers of individual disease status that can be easily computed in new patients and data sets and are readily comparable with other continuous or categorical solutions.

Importantly, the present results complement modern efforts to derive transdiagnostic biotypes. For instance, Clementz et al used comprehensive neurocognitive and neurophysiological data to identify 3 discrete biotypes across the schizophrenia spectrum (bipolar, schizoaffective, and schizophrenia).[34] A subsequent voxel-based morphometry study showed that biotype 1 with poor cognitive-sensory function had a broadly distributed cortical and subcortical volume reduction, while biotype 2 with moderate cognitive impairments exhibited more regional volume reduction within the insula and fronto-temporal regions.[83] Transdiagnostic symptom dimensions have been identified in the same data set, with more severe negative symptoms for biotypes 1 and 2[84]. Our findings enrich insights from this work, showing a dimensional clinical (cognitive-negative) and neuroanatomical pattern that effectively bridges biotypes 1 and 2. Consistent with Reininghaus et al,[84] the present study demonstrates successful integration of phenomenological and neuroimaging data to identify dimensional characteristics of schizophrenia. Altogether, the identified clinical-anatomical dimension can be readily applied in concert with categorical biotypes to advance progress in treatment development and diagnostics across the schizophrenia spectrum.[34,35,83]

Default mode and visual networks—anchors of the cognitive-negative dimension

In the present model, the dominant cognitive-negative dimension was most closely related to deformation in the default mode and visual networks. Our group and others have recently demonstrated that deformation topography in schizophrenia reflects anatomical and functional network topology, with core deficits observed in the default mode network.[13,22,23] For instance, Wannan et al observed a similar network-based pattern of brain abnormalities across multiple stages of the schizophrenia spectrum (from first episode to chronic and treatment-resistant patients).[22] In addition, using a transdiagnostic approach (schizophrenia, bipolar disorder, and relatives) Stan et al demonstrated that psychotic symptoms are related to a regional pattern within the heteromodal cortex.[85] The present findings extend this work by showing that network-based deformation can be mapped to a cognitive-negative dimension.

Previous case-control studies revealed that clinical subtypes with predominantly negative symptoms[86] and biotypes with cognitive-sensory impairments[83] demonstrated most extensive cortical thinning and global gray matter reduction, respectively. At the same time, localized associations have been reported for cognitive function and

volume reduction in the anterior cingulate, insula, hippocampus/parahippocampal gyrus, middle frontal gyrus, and cognitive function,[18,19] as well as negative symptoms and reduced orbitofrontal cortical thickness.[17] The present report builds on these findings, demonstrating that a cognitive-negative dimension of schizophrenia reflects targeted abnormalities in spatially specific networks.

More generally, these results shed new light on how pathological processes of brain structure and function are intertwined.[10,21,87] An emerging literature points to a continuous unimodal–transmodal cortical synaptic hierarchy,[88,89] manifesting as smooth topographic gradients of gene transcription,[90,91] intracortical myelin,[92,93] cortical thickness,[94] excitation–inhibition balance,[95] and macroscale structural and functional connectivity.[69,96–98] Our results show that the dominant cognitive-negative dimension originates from the ends or "anchors" of this hierarchy: the visual[15,99] and default mode networks.[100–102] This raises the possibility that multiple pathological processes, originating from opposing ends of the putative sensory-fugal hierarchy, may be involved in the disease. Interestingly, 2 recent functional imaging studies found evidence of atypical functional connectivity and integration between unimodal and transmodal cortices.[103,104] Our results show that these deficits in functional coordination may ultimately originate from underlying anatomical abnormalities, reflecting large-scale molecular and cellular gradients.

Limitations and Future Directions

The present report highlights a latent clinical-anatomical dimension of schizophrenia, but the findings should be interpreted with respect to several important limitations. First, data-driven multivariate models seek to map multiple modalities to one another but, as a result, they cannot be used to make inferences about localized relationships between specific clinical symptoms and specific brain regions. Second, the present findings are based on cross-sectional data, precluding the extrapolation of longitudinal progression. In addition, there is consistent evidence for 5 specific psychosis domains of positive, negative, disorganized, manic, and depressive symptoms across the schizophrenia spectrum.[84] The current study was based on data sets assessing psychotic symptoms with the SAPS and SANS, which limited the ability to investigate clinical-anatomical dimensions in the presence of more comprehensive psychopathological measures of the affective domain (mania and depression) and disorganization domain. Future work should extend the present findings and study dimensional multivariate brain-behavior relationships across the psychosis continuum, trans-diagnostically (eg, schizophrenia-schizoaffective-bipolar disorders) and across different biotypes, including comprehensive psychopathological and neurocognitive data.[34,38,59]

In terms of methodology, it is important to note that head motion could systematically bias structural MRI.[105–108] Addressing this potential confound would require additional in-scanner head-motion estimates from functional MRI (fMRI),[106,108] which were not available in either data set. Finally, the influence of drug exposure on brain structure is another important confounding factor that is challenging to address in cross-sectional studies. We found no evidence of an association between current medication dose and the clinical-anatomical dimensions in a subsample (n = 87) of the discovery data set. However, these results are limited by the fact that current medication does not allow conclusions to be drawn on long-term drug exposure. Future studies in longitudinal data are warranted to explore medication effects on latent clinical-anatomical dimensions.

Conclusion

The present work contributes to a growing recognition that individual clinical symptoms do not occur in isolation, nor can they be precisely mapped to a single locus in complex disorders, such as schizophrenia. An integrated multivariate model allows clinical experience and objective neuroanatomical measurements to simultaneously inform one another, yielding a more holistic understanding of heterogeneity in the patient population. The clinical-anatomical dimension identified here opens a new direction for dimensional stratification, complementing existing efforts to develop sensitive diagnostics and individualized treatment strategies.

Supplementary Material

Supplementary material is available at *Schizophrenia Bulletin*.

Funding

This research was undertaken thanks in part to funding from the Canada First Research Excellence Fund, awarded to McGill University for the Healthy Brains for Healthy Lives initiative. M.K. acknowledges support from the National Bank Fellowship (McGill University) and the Swiss National Foundation (P2SKP3_178175). B.M. acknowledges support from the Natural Sciences and Engineering Research Council of Canada (Discovery Grant RGPIN #017-04265) and from the Fonds de Recherche du Québec - Santé (Chercheur Boursier). G.S. acknowledges support from the Natural Sciences and Engineering Research Council of Canada and from the Healthy Brains for Healthy Lives initiative at McGill University. C.M. acknowledges support from the Canadian Institutes of Health Research. Data collection and sharing for this project was funded by National Institute of Mental Health grant 1R01 MH084803.

Data Availability Statement

Deformation patterns of the clinical-anatomical dimensions are freely available for visualization and download for further exploration and future research from Neurovault (https://identifiers.org/neurovault.collection:6825).

References

1. Rosengard RJ, Malla A, Mustafa S, et al. Association of preonset subthreshold psychotic symptoms with longitudinal outcomes during treatment of a first episode of psychosis. *JAMA Psychiatry.* 2019;76(1):61–70.
2. Hovington CL, Bodnar M, Joober R, Malla AK, Lepage M. Identifying persistent negative symptoms in first episode psychosis. *BMC Psychiatry.* 2012;12:224.
3. Austin SF, Mors O, Budtz-Jørgensen E, et al. Long-term trajectories of positive and negative symptoms in first episode psychosis: a 10-year follow-up study in the OPUS cohort. *Schizophr Res.* 2015;168(1–2):84–91.
4. Kahn RS, Keefe RS. Schizophrenia is a cognitive illness: time for a change in focus. *JAMA Psychiatry.* 2013;70(10):1107–1112.
5. Bobes J, Arango C, Garcia-Garcia M, Rejas J; CLAMORS Study Collaborative Group. Prevalence of negative symptoms in outpatients with schizophrenia spectrum disorders treated with antipsychotics in routine clinical practice: findings from the CLAMORS study. *J Clin Psychiatry.* 2010;71(3):280–286.
6. Chang WC, Ho RWH, Tang JYM, et al. Early-stage negative symptom trajectories and relationships with 13-year outcomes in first-episode nonaffective psychosis. *Schizophr Bull.* 2019;45(3):610–619.
7. Milev P, Ho BC, Arndt S, Andreasen NC. Predictive values of neurocognition and negative symptoms on functional outcome in schizophrenia: a longitudinal first-episode study with 7-year follow-up. *Am J Psychiatry.* 2005;162(3):495–506.
8. Shamsi S, Lau A, Lencz T, et al. Cognitive and symptomatic predictors of functional disability in schizophrenia. *Schizophr Res.* 2011;126(1–3):257–264.
9. Austin SF, Mors O, Secher RG, et al. Predictors of recovery in first episode psychosis: the OPUS cohort at 10 year follow-up. *Schizophr Res.* 2013;150(1):163–168.
10. Frangou S. A systems neuroscience perspective of schizophrenia and bipolar disorder. *Schizophr Bull.* 2014;40(3):523–531.
11. Meda SA, Ruaño G, Windemuth A, et al. Multivariate analysis reveals genetic associations of the resting default mode network in psychotic bipolar disorder and schizophrenia. *Proc Natl Acad Sci USA.* 2014;111(19):E2066–E2075.
12. Dong D, Wang Y, Chang X, Luo C, Yao D. Dysfunction of large-scale brain networks in schizophrenia: a meta-analysis of resting-state functional connectivity. *Schizophr Bull.* 2018;44(1):168–181.
13. Cauda F, Nani A, Manuello J, et al. Brain structural alterations are distributed following functional, anatomic and genetic connectivity. *Brain.* 2018;141(11):3211–3232.
14. Erp TG van, Hibar DP, Rasmussen JM, et al. Subcortical brain volume abnormalities in 2028 individuals with schizophrenia and 2540 healthy controls via the enigma consortium. *Mol Psychiatry.* 2016;21(4):547.
15. van Erp TGM, Walton E, Hibar DP, et al.; Karolinska Schizophrenia Project. Cortical brain abnormalities in 4474 individuals with schizophrenia and 5098 control subjects via the Enhancing Neuro Imaging Genetics Through Meta Analysis (ENIGMA) Consortium. *Biol Psychiatry.* 2018;84(9):644–654.
16. Kelly S, Jahanshad N, Zalesky A, et al. Widespread white matter microstructural differences in schizophrenia across 4322 individuals: results from the ENIGMA Schizophrenia DTI Working Group. *Mol Psychiatry.* 2018;23(5):1261–1269.
17. Walton E, Hibar DP, van Erp TGM, et al.; Karolinska Schizophrenia Project Consortium. Prefrontal cortical thinning links to negative symptoms in schizophrenia via the ENIGMA consortium. *Psychol Med.* 2018;48(1):82–94.
18. Czepielewski LS, Wang L, Gama CS, Barch DM. The relationship of intellectual functioning and cognitive performance to brain structure in schizophrenia. *Schizophr Bull.* 2017;43(2):355–364.
19. Woodward ND, Heckers S. Brain structure in neuropsychologically defined subgroups of schizophrenia and psychotic bipolar disorder. *Schizophr Bull.* 2015;41(6):1349–1359.
20. Walton E, Hibar DP, van Erp TG, et al.; Karolinska Schizophrenia Project Consortium. Positive symptoms associate with cortical thinning in the superior temporal gyrus via the ENIGMA Schizophrenia consortium. *Acta Psychiatr Scand.* 2017;135(5):439–447.
21. Fornito A, Zalesky A, Breakspear M. The connectomics of brain disorders. *Nat Rev Neurosci.* 2015;16(3):159–172.
22. Wannan CMJ, Cropley VL, Chakravarty MM, et al. Evidence for network-based cortical thickness reductions in schizophrenia. *Am J Psychiatry.* 2019;176(7):552–563.
23. Shafiei G, Markello RD, Makowski C, et al. Spatial patterning of tissue volume loss in schizophrenia reflects brain network architecture. *Biol Psychiatry.* 2020;87(8):727–735.
24. Palaniyappan L, Mallikarjun P, Joseph V, White TP, Liddle PF. Regional contraction of brain surface area involves three large-scale networks in schizophrenia. *Schizophr Res.* 2011;129(2-3):163–168.
25. Palaniyappan L. Progressive cortical reorganisation: a framework for investigating structural changes in schizophrenia. *Neurosci Biobehav Rev.* 2017;79:1–13.
26. Smith SM, Nichols TE, Vidaurre D, et al. A positive-negative mode of population covariation links brain connectivity, demographics and behavior. *Nat Neurosci.* 2015;18(11):1565–1567.
27. Miller KL, Alfaro-Almagro F, Bangerter NK, et al. Multimodal population brain imaging in the UK Biobank prospective epidemiological study. *Nat Neurosci.* 2016;19(11):1523–1536.
28. Zeighami Y, Fereshtehnejad SM, Dadar M, et al. A clinical-anatomical signature of Parkinson's disease identified with partial least squares and magnetic resonance imaging. *Neuroimage.* 2019;190:69–78.
29. Drysdale AT, Grosenick L, Downar J, et al. Resting-state connectivity biomarkers define neurophysiological subtypes of depression. *Nat Med.* 2017;23(1):28–38.
30. Xia CH, Ma Z, Ciric R, et al. Linked dimensions of psychopathology and connectivity in functional brain networks. *Nat Commun.* 2018;9(1):3003.
31. Moser DA, Doucet GE, Lee WH, et al. Multivariate associations among behavioral, clinical, and multimodal imaging phenotypes in patients with psychosis. *JAMA Psychiatry.* 2018;75(4):386–395.

32. Zheng YQ, Zhang Y, Yau Y, et al. Local vulnerability and global connectivity jointly shape neurodegenerative disease propagation. *PLoS Biol.* 2019;17(11):e3000495.
33. Mišić B, Sporns O. From regions to connections and networks: new bridges between brain and behavior. *Curr Opin Neurobiol.* 2016;40:1–7.
34. Clementz BA, Sweeney JA, Hamm JP, et al. Identification of distinct psychosis biotypes using brain-based biomarkers. *Am J Psychiatry.* 2016;173(4):373–384.
35. Chand GB, Dwyer DB, Erus G, et al. Two distinct neuroanatomical subtypes of schizophrenia revealed using machine learning. *Brain.* 2020;143(3):1027–1038.
36. Cuthbert BN, Insel TR. Toward new approaches to psychotic disorders: the NIMH Research Domain Criteria project. *Schizophr Bull*. 2010;36(6):1061–1062.
37. Cuthbert BN. The RDoC framework: facilitating transition from ICD/DSM to dimensional approaches that integrate neuroscience and psychopathology. *World Psychiatry.* 2014;13(1):28–35.
38. van Os J, Kapur S. Schizophrenia. *Lancet*. 2009;374(9690):635–645.
39. van Os J, Kenis G, Rutten BP. The environment and schizophrenia. *Nature.* 2010;468(7321):203–212.
40. Barch DM, Bustillo J, Gaebel W, et al. Logic and justification for dimensional assessment of symptoms and related clinical phenomena in psychosis: relevance to DSM-5. *Schizophr Res.* 2013;150(1):15–20.
41. Reed GM, First MB, Kogan CS, et al. Innovations and changes in the ICD-11 classification of mental, behavioural and neurodevelopmental disorders. *World Psychiatry.* 2019;18(1):3–19.
42. Kogan A, Alpert K, Ambite JL, Marcus DS, Wang L. Northwestern University schizophrenia data sharing for SchizConnect: a longitudinal dataset for large-scale integration. *Neuroimage.* 2016;124(Pt B):1196–1201.
43. Cardenas VA, Boxer AL, Chao LL, et al. Deformation-based morphometry reveals brain atrophy in frontotemporal dementia. *Arch Neurol.* 2007;64(6):873–877.
44. Chung MK, Worsley KJ, Paus T, et al. A unified statistical approach to deformation-based morphometry. *Neuroimage.* 2001;14(3):595–606.
45. Leow AD, Klunder AD, Jack CR Jr, et al.; ADNI Preparatory Phase Study. Longitudinal stability of MRI for mapping brain change using tensor-based morphometry. *Neuroimage.* 2006;31(2):627–640.
46. Studholme C, Cardenas V, Blumenfeld R, et al. Deformation tensor morphometry of semantic dementia with quantitative validation. *Neuroimage.* 2004;21(4):1387–1398.
47. Zeighami Y, Ulla M, Iturria-Medina Y, et al. Network structure of brain atrophy in de novo Parkinson's disease. *eLife.* 2015;4:e08440.
48. Avants BB, Tustison NJ, Song G, Cook PA, Klein A, Gee JC. A reproducible evaluation of ANTs similarity metric performance in brain image registration. *Neuroimage.* 2011;54(3):2033–2044.
49. McIntosh AR, Lobaugh NJ. Partial least squares analysis of neuroimaging data: applications and advances. *Neuroimage.* 2004;23(suppl 1):S250–S263.
50. Krishnan A, Williams LJ, McIntosh AR, Abdi H. Partial least squares (PLS) methods for neuroimaging: a tutorial and review. *Neuroimage.* 2011;56(2):455–475.
51. McIntosh AR, Mišić B. Multivariate statistical analyses for neuroimaging data. *Annu Rev Psychol.* 2013;64:499–525.
52. Andreasen NC. *Scale for the Assessment of Positive Symptoms (SAPS)*. Iowa City, IA: University of Iowa; 1984.
53. Andreasen NC. *The Scale for the Assessment of Negative Symptoms (SANS)*. Iowa City, IA: University of Iowa; 1983.
54. Kotov R, Foti D, Li K, Bromet EJ, Hajcak G, Ruggero CJ. Validating dimensions of psychosis symptomatology: neural correlates and 20-year outcomes. *J Abnorm Psychol.* 2016;125(8):1103–1119.
55. Strauss GP, Horan WP, Kirkpatrick B, et al. Deconstructing negative symptoms of schizophrenia: avolition-apathy and diminished expression clusters predict clinical presentation and functional outcome. *J Psychiatr Res.* 2013;47(6):783–790.
56. Chouinard G. New nomenclature for drug-induced movement disorders including tardive dyskinesia. *J Clin Psychiatry.* 2004;65(suppl 9):9–15.
57. Chouinard G, Margolese HC. Manual for the Extrapyramidal Symptom Rating Scale (ESRS). *Schizophr Res.* 2005;76(2–3):247–265.
58. Wechsler D. *Wechsler Adult Intelligence Scale-III*. San Antonio, TX: The Psychological Corporation; 1997.
59. Tamminga CA, Ivleva EI, Keshavan MS, et al. Clinical phenotypes of psychosis in the Bipolar-Schizophrenia Network on Intermediate Phenotypes (B-SNIP). *Am J Psychiatry.* 2013;170(11):1263–1274.
60. Hudgens-Haney ME, Clementz BA, Ivleva EI, et al. Cognitive impairment and diminished neural responses constitute a biomarker signature of negative symptoms in psychosis. *Schizophr Bull.* 2020;46(5):1269–1281.
61. Ashburner J, Hutton C, Frackowiak R, Johnsrude I, Price C, Friston K. Identifying global anatomical differences: deformation-based morphometry. *Hum Brain Mapp.* 1998;6(5–6):348–357.
62. Béland S, Makowski C, Konsztowicz S, Buchy L, Chakravarty MM, Lepage M. Clarifying associations between cortical thickness, subcortical structures, and a comprehensive assessment of clinical insight in enduring schizophrenia. *Schizophr Res.* 2019;204:245–252.
63. Edgington E, Onghena P. *Randomization Tests*. Boca Raton, FL: Chapman and Hall/CRC; 2007.
64. Efron B, Tibshirani R. Bootstrap methods for standard errors, confidence intervals, and other measures of statistical accuracy. *Stat Sci.* 1986;1(1):54–75.
65. Mirchi N, Betzel RF, Bernhardt BC, Dagher A, Mišic B. Tracking mood fluctuations with functional network patterns. *Soc Cogn Affect Neurosci.* 2019;14(1):47–57.
66. Kovacevic N, Abdi H, Beaton D, McIntosh AR. Revisiting pls resampling: Comparing significance versus reliability across range of simulations. In: *New Perspectives in Partial Least Squares and Related Methods*. New York, NY: Springer; 2013: 159–170.
67. Alexander-Bloch AF, Shou H, Liu S, et al. On testing for spatial correspondence between maps of human brain structure and function. *Neuroimage.* 2018;178:540–551.
68. Yeo BT, Krienen FM, Sepulcre J, et al. The organization of the human cerebral cortex estimated by intrinsic functional connectivity. *J Neurophysiol.* 2011;106(3):1125–1165.
69. Vázquez-Rodríguez B, Suárez LE, Markello RD, et al. Gradients of structure-function tethering across neocortex. *Proc Natl Acad Sci USA.* 2019;116(42):21219–21227.

70. Werner S, Malaspina D, Rabinowitz J. Socioeconomic status at birth is associated with risk of schizophrenia: population-based multilevel study. *Schizophr Bull.* 2007;33(6):1373–1378.
71. Goldberg S, Fruchter E, Davidson M, Reichenberg A, Yoffe R, Weiser M. The relationship between risk of hospitalization for schizophrenia, SES, and cognitive functioning. *Schizophr Bull.* 2011;37(4):664–670.
72. Smith G, Malla A, Williams R, Kopala L, Love L, Balshaw R. The Canadian national outcomes measurement study in schizophrenia: overview of the patient sample and methodology. *Acta Psychiatr Scand.* 2006;113:4–11.
73. Ran MS, Yang LH, Liu YJ, et al. The family economic status and outcome of people with schizophrenia in Xinjin, Chengdu, China: 14-year follow-up study. *Int J Soc Psychiatry.* 2017;63(3):203–211.
74. Samele C, van Os J, McKenzie K, et al.; UK700 Group. Does socioeconomic status predict course and outcome in patients with psychosis? *Soc Psychiatry Psychiatr Epidemiol.* 2001;36(12):573–581.
75. Martin JL, McLean G, Park J, et al. Impact of socioeconomic deprivation on rate and cause of death in severe mental illness. *BMC Psychiatry.* 2014;14:261.
76. Hackman DA, Farah MJ, Meaney MJ. Socioeconomic status and the brain: mechanistic insights from human and animal research. *Nat Rev Neurosci.* 2010;11(9):651–659.
77. Raizada RD, Richards TL, Meltzoff A, Kuhl PK. Socioeconomic status predicts hemispheric specialisation of the left inferior frontal gyrus in young children. *Neuroimage.* 2008;40(3):1392–1401.
78. Carpenter WT Jr, Heinrichs DW, Alphs LD. Treatment of negative symptoms. *Schizophr Bull.* 1985;11(3):440–452.
79. Kirschner M, Aleman A, Kaiser S. Secondary negative symptoms—a review of mechanisms, assessment and treatment. *Schizophr Res.* 2017;186:29–38.
80. Hartmann-Riemer MN, Hager OM, Kirschner M, et al. The association of neurocognitive impairment with diminished expression and apathy in schizophrenia. *Schizophr Res.* 2015;169(1–3):427–432.
81. Fervaha G, Foussias G, Agid O, Remington G. Motivational and neurocognitive deficits are central to the prediction of longitudinal functional outcome in schizophrenia. *Acta Psychiatr Scand.* 2014;130(4):290–299.
82. Harvey PD, Koren D, Reichenberg A, Bowie CR. Negative symptoms and cognitive deficits: what is the nature of their relationship? *Schizophr Bull.* 2006;32(2):250–258.
83. Ivleva EI, Clementz BA, Dutcher AM, et al. Brain structure biomarkers in the psychosis biotypes: findings from the bipolar-schizophrenia network for intermediate phenotypes. *Biol Psychiatry.* 2017;82(1):26–39.
84. Reininghaus U, Böhnke JR, Chavez-Baldini U, et al. Transdiagnostic dimensions of psychosis in the Bipolar-Schizophrenia Network on Intermediate Phenotypes (B-SNIP). *World Psychiatry.* 2019;18(1):67–76.
85. Stan AD, Tamminga CA, Han K, et al. Associating psychotic symptoms with altered brain anatomy in psychotic disorders using multidimensional item response theory models. *Cereb Cortex.* 2020;30(5):2939–2947.
86. Nenadic I, Yotter RA, Sauer H, Gaser C. Patterns of cortical thinning in different subgroups of schizophrenia. *Br J Psychiatry.* 2015;206(6):479–483.
87. Suárez LE, Markello RD, Betzel RF, Misic B. Linking structure and function in macroscale brain networks. *Trends Cogn Sci.* 2020;24(4):302–315.
88. Jones EG, Powell TP. An anatomical study of converging sensory pathways within the cerebral cortex of the monkey. *Brain.* 1970;93(4):793–820.
89. Mesulam MM. From sensation to cognition. *Brain.* 1998;121 (Pt 6):1013–1052.
90. Fulcher BD, Murray JD, Zerbi V, Wang XJ. Multimodal gradients across mouse cortex. *Proc Natl Acad Sci USA.* 2019;116(10):4689–4695.
91. Burt JB, Demirtaş M, Eckner WJ, et al. Hierarchy of transcriptomic specialization across human cortex captured by structural neuroimaging topography. *Nat Neurosci.* 2018;21(9):1251–1259.
92. Huntenburg JM, Bazin PL, Goulas A, Tardif CL, Villringer A, Margulies DS. A systematic relationship between functional connectivity and intracortical myelin in the human cerebral cortex. *Cereb Cortex.* 2017;27(2):981–997.
93. Paquola C, Vos De Wael R, Wagstyl K, et al. Microstructural and functional gradients are increasingly dissociated in transmodal cortices. *PLoS Biol.* 2019;17(5):e3000284.
94. Wagstyl K, Ronan L, Goodyer IM, Fletcher PC. Cortical thickness gradients in structural hierarchies. *Neuroimage.* 2015;111:241–250.
95. Wang XJ. Macroscopic gradients of synaptic excitation and inhibition in the neocortex. *Nat Rev Neurosci.* 2020;21(3):169–178.
96. Margulies DS, Ghosh SS, Goulas A, et al. Situating the default-mode network along a principal gradient of macroscale cortical organization. *Proc Natl Acad Sci USA.* 2016;113(44):12574–12579.
97. Baum GL, Cui Z, Roalf DR, et al. Development of structure-function coupling in human brain networks during youth. *Proc Natl Acad Sci USA.* 2020;117(1):771–778.
98. Vazquez-Rodriguez B, Liu Z-Q, Hagmann P, Misic B. Signal propagation via cortical hierarchies. *Netw. Neurosci.* 2020;1–30. doi: 10.1162/netn_a_00153.
99. Vieira S, Gong Q, Scarpazza C, et al. Neuroanatomical abnormalities in first-episode psychosis across independent samples: a multi-centre mega-analysis [published online ahead of print December 20, 2019]. *Psychol Med.* 2019;1–11. doi:10.1017/S0033291719003568.
100. Jimenez AM, Riedel P, Lee J, Reavis EA, Green MF. Linking resting-state networks and social cognition in schizophrenia and bipolar disorder. *Hum Brain Mapp.* 2019;40(16):4703–4715.
101. Abram SV, Wisner KM, Fox JM, et al. Fronto-temporal connectivity predicts cognitive empathy deficits and experiential negative symptoms in schizophrenia. *Hum Brain Mapp.* 2017;38(3):1111–1124.
102. Hare SM, Ford JM, Mathalon DH, et al. Salience-default mode functional network connectivity linked to positive and negative symptoms of schizophrenia. *Schizophr Bull.* 2019;45(4):892–901.
103. Cao H, Zhou H, Cannon TD. Functional connectome-wide associations of schizophrenia polygenic risk [published online ahead of print March 3, 2020]. *Mol Psychiatry.* 2020. doi:10.1038/s41380-020-0699-3.
104. Dong D, Yao D, Wang Y, et al. Altered sensorimotor-to-transmodal hierarchical organization in schizophrenia. *bioRxiv.* 2020. doi:10.1101/2020.03.06.980607.
105. Reuter M, Tisdall MD, Qureshi A, Buckner RL, van der Kouwe AJW, Fischl B. Head motion during MRI acquisition reduces gray matter volume and thickness estimates. *Neuroimage.* 2015;107:107–115.

106. Alexander-Bloch A, Clasen L, Stockman M, et al. Subtle in-scanner motion biases automated measurement of brain anatomy from in vivo MRI. *Hum Brain Mapp.* 2016;37(7):2385–2397.
107. Rosen AFG, Roalf DR, Ruparel K, et al. Quantitative assessment of structural image quality. *Neuroimage.* 2018;169:407–418.
108. Savalia NK, Agres PF, Chan MY, Feczko EJ, Kennedy KM, Wig GS. Motion-related artifacts in structural brain images revealed with independent estimates of in-scanner head motion. *Hum Brain Mapp.* 2017;38(1):472–492.
109. Eckart C, Young G. The approximation of one matrix by another of lower rank. *Psychometrika.* 1936;1(3):211–218.
110. Rahim M, Thirion B, Varoquaux G. Multi-output predictions from neuroimaging: assessing reduced-rank linear models. In: 2017 International Workshop on Pattern Recognition in Neuroimaging (PRNI), Toronto, ON, 2017, pp. 1–4. doi:10.1109/PRNI.2017.7981504.